







Time-resolved shot-by-shot photoelectron spectroscopy of autoionizing Xe⁺ states by EUV-free-electron-laser and near-IR laser pulses

Mizuho Fushitani ^{1,2,*} Yoshitaka Kawabe ¹ Hikaru Fujise,¹ Makoto Yamada,¹ Hiroka Hasegawa ¹ Shigeki Owada,^{2,3} Tadashi Togashi,^{2,3} Kyo Nakajima,^{2,3} Makina Yabashi,^{2,3} Akitaka Matsuda ^{1,2} Yasumasa Hikosaka ^{2,4} and Akiyoshi Hishikawa ^{1,2,5,†}

¹Graduate School of Science, Nagoya University, Furo-cho, Chikusa, Nagoya, Aichi, 464-8602, Japan

²RIKEN SPring-8 Center, 1-1-1 Koto, Sayo-cho, Sayo-gun, Hyogo, 679-5148, Japan

³Japan Synchrotron Radiation Research Institute, 1-1-1 Koto, Sayo-cho, Sayo-gun, Hyogo, 679-5198, Japan

⁴Institute of Liberal Arts and Sciences, University of Toyama, 2630 Sugitani, Toyama, Toyama, 930-0194, Japan

⁵Research Center for Materials Science, Nagoya University, Furo-cho, Chikusa, Nagoya, Aichi, 464-8602, Japan



(Received 15 May 2021; accepted 20 July 2021; published 6 August 2021)

Ultrafast dynamics of highly excited Rydberg states of Xe⁺ is investigated by time-resolved shot-by-shot photoelectron spectroscopy with EUV-free-electron-laser pump (40.8 eV) and near-infrared probe (1.56 eV) pulses. Sorting the single-shot spectra in the order of relative delay between the two pulses allows for investigating ultrafast decays of intermediate states participating in the double ionization of Xe. Observed photoelectron spectra show a biexponential decay within ~ 100 fs and ~ 300 ps in addition to constant signals lasting longer than 1 ns. These ultrafast decays reflect the lifetimes of autoionizing Rydberg states converging to electronically excited states of Xe²⁺. The results demonstrate that time-resolved shot-by-shot EUV-free-electron-laser photoelectron spectroscopy with a synchronized optical laser provides a powerful tool for investigating ultrafast electron emission processes.

DOI: [10.1103/PhysRevA.104.023102](https://doi.org/10.1103/PhysRevA.104.023102)

I. INTRODUCTION

Double ionization is one of the fundamental physical processes that can occur when isolated atomic as well as molecular systems acquire energies larger than the second ionization threshold by interactions with photons [1,2] or high-energy particles [3,4]. Among others, single-photon double ionization of neutral atoms and molecules has attracted considerable attention since photoemission of two electrons is forbidden under single-active-electron approximation so that electronic correlations play a key role in two-electron processes [5]. Two emitted electrons show characteristic correlations, depending on whether the double ionization proceeds in the direct or indirect pathways. In the direct pathway where two electrons are simultaneously emitted, the extra energy in double ionization is shared by the electrons, leading to a broad structureless photoelectron spectrum, while the angular distribution of photoelectrons provides detailed information on how they correlate to form an electron-pair wave function in continuum states [6,7].

When double ionization of atoms and molecules takes place indirectly, i.e., via an intermediate state, each electron is ejected with a specific kinetic energy; one electron has a kinetic energy determined by the difference between the photon energy and the energy of the intermediate state while the other electron is emitted with an energy corresponding to

the difference between the intermediate and final states. As the intermediate state is located within the ionization continuum of singly charged ions, the second photoemission takes place through a coupling between the discrete intermediate state and the electronic continuum (autoionization), and competes with other processes such as radiative and dissociative decays, depending on the timescale of these processes.

The timescale of these electron emission processes can be obtained from spectral widths of the corresponding photoelectron peaks. When the electron emission occurs on a timescale of a few femtoseconds, the spectral width appears on the order of several hundreds of a meV, which is large enough to be precisely determined by conventional photoelectron spectrometers, as demonstrated for Auger decays of Ar, Kr, and Xe [8,9]. However, such a precise measurement of the natural line width is often limited when a target quantum state undergoes slow relaxation processes with a lifetime larger than 1 picosecond, whose spectral width becomes as narrow as 1 meV or below.

Double ionization of Xe atoms has been investigated by various spectroscopic techniques as in the simple two-electron systems such as He [4,10] and H₂ [11,12]. High-resolution photoelectron studies [13–18] have identified sharp peaks reflecting autoionizing states above the lowest threshold of Xe²⁺(³P₂). Strong peak progressions are assigned to the (¹D)nd (²S_{1/2}) Rydberg series (*n* stands for the principal quantum number) converging to the Xe²⁺(¹D₂) state [17] although other weak peaks remain unassigned. Eland *et al.* studied double ionization of Xe by electron-electron coincidence measurements with a He II light source and revealed signifi-

*fushitani@chem.nagoya-u.ac.jp

†hishi@chem.nagoya-u.ac.jp

cant contributions of autoionizing states to the single-photon double ionization processes [19]. Angular distribution measurements revealed the preference of two electron emissions in opposite directions to each other for the direct pathway [20,21]. Time-resolved electron momentum imaging spectroscopy was applied to Xe to clarify angular correlations for the direct and indirect pathways of multiphoton double ionization [22,23]. The timescale of the direct double ionization of Xe was also interrogated by using attosecond photoelectron spectroscopy [24], which showed that two-electron emission to the 1D_2 state of Xe^{2+} occurs with a delay of 55 as, compared to photoemission by single ionization to the 2P state of Xe^+ . On the other hand, much less information is available on the dynamics of the indirect pathway via autoionizing states. In Refs. [22,23], time-resolved studies of the Xe^{2+} ion yield were also carried out, which showed a step-function-like increase with the timescale reflecting temporal widths of pump and probe pulses. One may discuss the decay of autoionizing states from the associated spectral widths [19], but precise estimation was difficult to make due to the limitation of instrumental resolution. As in other atoms and molecules, autoionization states have various decay times depending on how they are coupled to the electron continuum.

Pump and probe experiments using synchrotron radiation and optical lasers have been carried out to study decay processes of autoionizing states [25–27]. A single autoionizing state can be selectively excited in such experiments, but the time resolution is limited to the picosecond or nanosecond range by the pulse duration of the synchrotron radiation. Free-electron lasers (FELs) in the extreme ultraviolet (EUV) and x-ray regions have been recognized as an ideal light source for studies on excitation and deexcitation processes of highly excited atomic and molecular states for their ultrashort pulse duration in the femtosecond range [28–31]. In spite of the pulse shortening, the time resolution is often limited to 1 ps due to the timing jitter between FEL and optical laser pulses, unless postcorrection methods [32–35] are employed.

Here, we carry out time-resolved photoelectron spectroscopy of the double ionization process of Xe occurring via indirect pathways by using EUV FEL and ultrashort near-infrared (NIR) laser pulses. By scanning the time delay between the two pulses on timescales from femtosecond to nanosecond, we have identified transient photoelectron signals characterized by two different time-decay components (~ 100 fs and ~ 300 ps), associated with highly excited Rydberg states of Xe^+ ions located above the second ionization threshold. In particular, in the measurements on the femtosecond timescale, we incorporate a timing monitor system [35] in shot-by-shot photoelectron spectroscopy [36] to improve the time resolution that is otherwise limited on the ps timescale due to the timing jitter [29,37]. The time resolution thus obtained can be less than 100 fs [35,38], depending on the pulse durations of the FEL and NIR lasers. The present time-resolved photoelectron measurements with the timing monitor system allow for investigating ultrafast dynamics of various materials occurring on the 100 fs timescale, as achieved by other jitter-free measurements with seeded FELs [39,40] and tabletop high-order harmonics pulses [22,23,41,42].

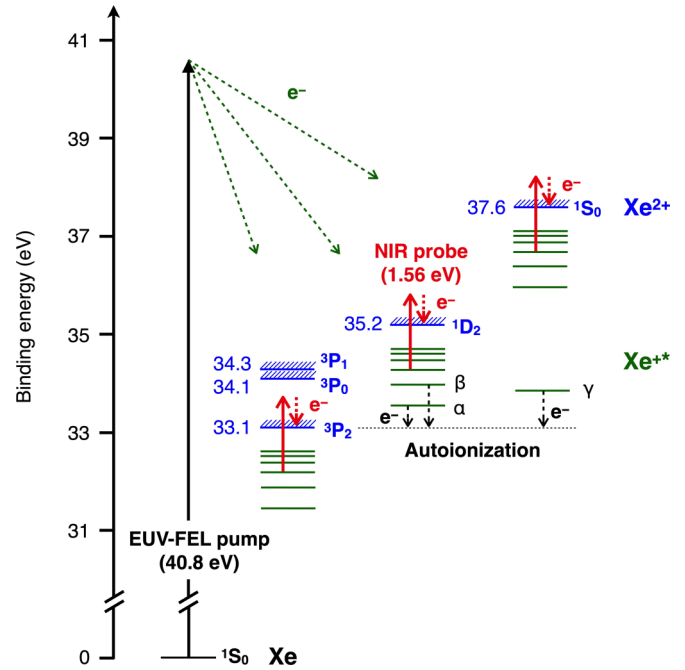


FIG. 1. Relevant energy levels of Xe, Xe^+ (green), and Xe^{2+} (blue) and schematics of EUV-pump (40.8 eV) and NIR-probe (1.56 eV) photoelectron spectroscopy of indirect double ionization of Xe. Among the 3P manifolds of Xe^{2+} , the NIR-probe process is indicated only for the 3P_2 level.

II. EXPERIMENT

The pump and probe scheme in the present study is depicted in Fig. 1. EUV-FEL pulses at 40.8 eV ionize Xe into Xe^+ in the ground and excited states. Excited states located at 31–38 eV are known to be $5s$ correlation satellites, and some of them are assigned to Rydberg series converging to the 3P , 1D , and 1S electronic states of Xe^{2+} [14,17]. Among others, the nd ($^2S_{1/2}$) Rydberg series converging to the Xe^{2+} (1D) state have dominant line intensities due to strong interactions of the electronic states in the $5s^{-1}$ configuration [17]. Time-delayed ultrashort NIR laser pulses promote those Rydberg states to the corresponding states of Xe^{2+} and thereby the relaxation processes of the Rydberg states of Xe^+ can be investigated.

Figure 2(a) illustrates a schematic of the experimental setup. Ultrashort EUV pulses (40.8 eV, ~ 30 fs, 60 Hz) from the soft x-ray beamline (BL1) at SACLA of RIKEN Harima institute in Japan were focused by a set of Kirkpatrick-Baez (KB) mirrors onto the sample gas (Xe or He) being introduced through a copper nozzle into an ultrahigh-vacuum chamber ($\sim 10^{-10}$ Torr). Ultrashort NIR laser pulses (1.56 eV, ~ 50 fs) which were synchronized with the FEL were focused on the same target by a planoconvex lens ($f = 1000$ mm) at an angle of $\sim 2^\circ$ with respect to the FEL. Beam diameters (FWHM: full width at half maximum) of EUV and NIR laser pulses were estimated to be ~ 6 and ~ 80 μm at the focus, respectively, and both pulses are horizontally polarized. Electrons produced by the laser irradiation were detected by using a magnetic bottle type photoelectron spectrometer [36] equipped with a retarding unit. Electron kinetic energies E were calibrated with Xe $4d$ Auger electron peaks [43] and autoionization peaks of

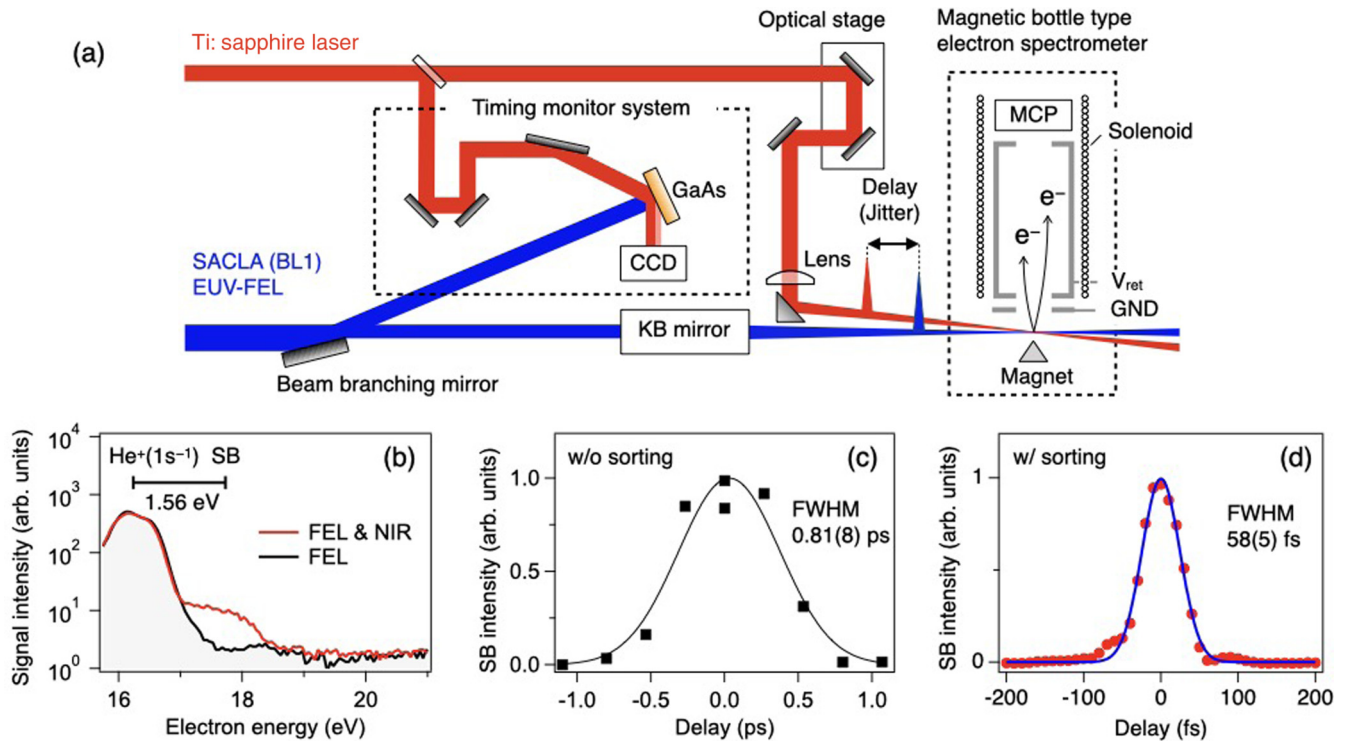


FIG. 2. (a) A schematic of the present experimental setup for time-resolved single-shot photoelectron spectroscopy using a magnetic bottle electron spectrometer. Timing monitor system provides information on relative delays between EUV-FEL and NIR laser pulses on the shot-by-shot basis, allowing us to improve the time resolution influenced by timing jitter. (b) Photoelectron spectra of He with [red (gray)] and without [black] NIR laser pulses. He $1s$ photoelectron peak and its sideband (SB) are indicated as sticks. (c) Integrated intensities of He $1s$ photoelectron sideband in (b) as a function of pump-probe delay without using a timing monitor system. Full width at half maximum (FWHM) corresponds to the intrinsic time resolution under the influence of the timing jitter. (d) Same as (c), but using the timing monitor system at $\Delta t = 0$ ps. Single-shot photoelectron spectra (9×10^3) are sorted in the order of delay and averaged in each time bin (10 fs) before the SB integration.

Xe⁺ [19]. A typical energy resolution ΔE was $E/\Delta E \sim 20$ for $E < 200$ eV while the uncertainty of E is estimated to be 0.1 eV for $E < 1$ eV in the current study.

The optical path length for the NIR laser line was controlled by using an optical stage, by which the time delay between the FEL and NIR laser pulses was introduced. Although the optical stage allows for the minimum delay of 6.7 fs, the time resolution is limited by fluctuations in synchronization (timing jitter). To evaluate the time resolution in the presence of the timing jitter, photoelectron sideband measurements of He were carried out as the photoelectron sideband can be formed only when the FEL and NIR laser pulses are overlapped in space and time [35]. Figure 2(b) shows the photoelectron spectrum of He atoms by using EUV-FEL and NIR laser pulses at the time delay of 0 ps with a retardation voltage of $V_{\text{ret}} = -15.5$ eV. The peak at 16.2 eV is attributed to He $1s$ photoelectron formed by single-photon ionization by EUV FEL while a sideband peak appears on the higher-energy side by an amount of photon energy (1.56 eV) of the NIR laser pulse. The integrated intensity of the sideband as a function of the time delay is plotted in Fig. 2(c). The least-squares fitting with a Gaussian function provides the FWHM of 0.81(8) ps, which corresponds to the time resolution in the presence of the timing jitter. The time zero was set to the maximum posi-

tion of the Gaussian envelope. The jitter-limited photoelectron measurements were carried out for relaxation dynamics of Xe⁺ occurring on the subnanosecond timescale.

To monitor faster relaxation on the subpicosecond timescale, we utilized the timing monitor system recently developed for the BL1 beamline [35]. The system was equipped with a visible charge-coupled device (CCD) camera to image a spatial profile of the reflectivity of NIR laser pulses from a gallium arsenide (GaAs) surface. An arrival timing between FEL and NIR laser pulses can be extracted for each shot from a position of a sudden drop of the NIR reflectivity due to FEL irradiation on GaAs. With this time information, single-shot photoelectron spectra were sorted in the order of relative delay times between FEL and NIR laser pulses. Figure 2(d) shows the time dependence of the sideband intensity of the He $1s$ photoelectron peak after sorting (10-fs binning). This time broadening provides the overall time resolution in the present measurement, which results from pulse durations of FEL and NIR as well as an uncertainty of the timing monitor system. The FWHM in Fig. 2(d) was obtained as 58(5) fs, thereby allowing us to investigate the target process with an order of magnitude better time resolution than that limited by jitter.

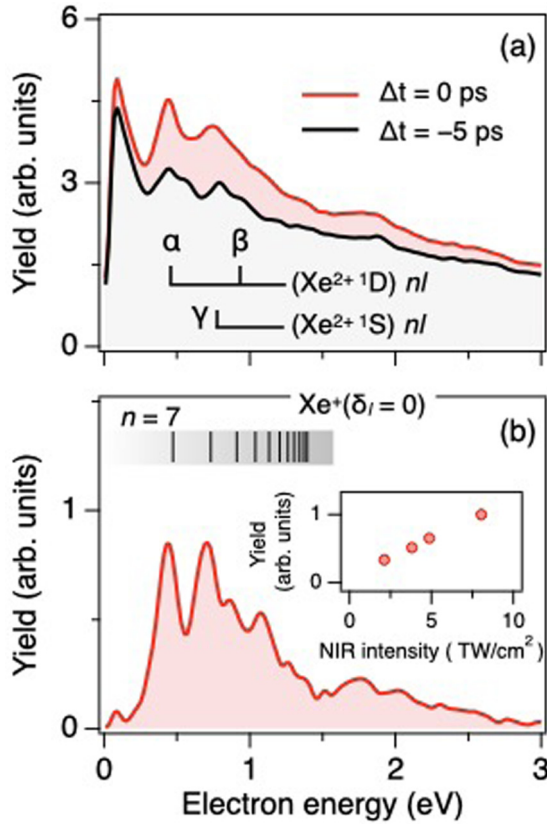


FIG. 3. (a) Photoelectron spectra of Xe with EUV-FEL pump (4×10^{13} W/cm²) and NIR probe (8×10^{12} W/cm²) pulses at pump-probe delay of $\Delta t = 0$ ps [red (gray)] and $\Delta t = -5$ ps (black). Sticks α , β , and γ are for electrons formed by autoionization indicated by Fig. 1. (b) The difference spectrum between them is displayed in the upper part. Stick spectra are calculated by using Eq. (1) with $\delta_l = 0$. Inset: NIR intensity dependence of the net photoelectron signals (0.3–1.6 eV) at $\Delta t = 0$ ps.

III. RESULTS AND DISCUSSION

Figure 3(a) shows photoelectron spectra of Xe by using EUV-FEL pump (4×10^{13} W/cm²) and NIR probe (8×10^{12} W/cm²) pulses. These photoelectron spectra were collected for 9×10^3 laser shots. The spectrum in black is obtained by averaging at the pump-probe time delay of $\Delta t = -5$ ps where NIR pulses precede FEL pulses. It exhibits clear peaks at 0.45, 0.79, and 0.93 eV, which can be attributed to electrons produced by autoionization of Rydberg states of Xe^{*+} [19] excited by FEL pulses (see Fig. 1). These autoionizing Rydberg states, α , β , and γ , were dominantly populated among the autoionizing states and assigned to Rydberg states, $(\text{Xe}^{2+} \ ^1D) \ 8d, 9d$, and $(\text{Xe}^{2+} \ ^1S) \ 7d$, in the previous study using a HeII light source [19], while the observed energies imply lower Rydberg states in the same manifold.

The pump-probe spectrum at $\Delta t = 0$ ps exhibits a substantial increase in intensity in the range of 0.3–3 eV. The distribution of the net increased signals can be clearly seen in the difference spectrum [Fig. 3(b)], obtained after subtraction of the spectrum at $\Delta t = -5$ ps. Several photoelectron peaks are identified in the range of 0.3–1.6 eV with a distribution

where signal intensities become weaker for higher-energy peaks.

The integrated intensities of the band between 0.3 and 1.6 eV at $\Delta t = 0$ ps as a function of the NIR intensity are plotted in the inset of Fig. 3(b). The electron signal linearly increases as the NIR intensity increases in the range of $2\text{--}8 \times 10^{12}$ W/cm². This NIR intensity dependence shows that ionization by the NIR laser pulse essentially occurs by single-photon process and that the photoelectron signal is related to the NIR single-photon ionization of Rydberg states near the ionization thresholds.

It should be noted that peaks seen in the range of 1.6–3 eV in Fig. 3(b) can be attributed to the above threshold ionization (ATI) from the same intermediate states related to the peaks of 0.3–1.6 eV. Although the ATI peaks are not spectrally resolved due the limited instrumental resolution, the energy positions appear to be shifted by the amount of NIR photon energy (1.56 eV) and the intensity distribution shows a similar tendency as those of peaks of 0.3–1.6 eV.

Assuming the single-photon ionization of the Rydberg series of Xe^+ , one can calculate photoelectron energy E by using the Rydberg formula for the effective core charge ($Z = 2$),

$$E = h\nu - Z^2 R_\infty / (n - \delta_l)^2, \quad (1)$$

where $h\nu$ is the NIR photon energy, R_∞ is the Rydberg constant, and δ_l is a quantum defect for series having an orbital angular momentum l . The photoelectron energies calculated with a quantum defect $\delta_l = 0$ show a good agreement with observed photoelectron peak energies [Fig. 3(b)]. This agreement suggests that the present Rydberg states are mainly associated with high l (≥ 3) series whose quantum defects are almost zero [44].

Figure 4(a) shows the difference photoelectron spectra as a function of time delay ranging from 0 to 1 ns, obtained by subtraction of the spectrum at $\Delta t = -5$ ps. As the time delay increases, photoelectron signals decrease in intensity, resulting in different peak distributions at $\Delta t > 600$ ps. To quantitatively discuss the decrease of the electron signals in Fig. 4(a), integrated intensities of selected peaks at 0.45, 0.71, 0.88, and 1.02 eV are plotted as a function of Δt in Fig. 4(b). Each curve shows a monotonic decay with a constant offset reflecting an additional lifetime contribution longer than 1 ns. By fitting a single exponential function to the data points, the decay constant (τ_1) is determined to be 190(30), 330(40), 210(50), and 260(60) ps for peaks at 0.45, 0.71, 0.88, and 1.02 eV, respectively. These curves clearly indicate that Rydberg states having subnanosecond lifetimes and those with much longer lifetimes are simultaneously promoted by EUV FEL.

Photoelectron signals lasting more than 1 ns have to be related to Rydberg states of Xe^+ lying below the lowest ionization threshold of $\text{Xe}^{2+}(\ ^3P_2)$, as such Rydberg states tend to relax through radiative processes where the lifetime is typically on the order of several nanoseconds as is observed for the $6d, 6d'$, and $7s$ states of Xe^+ [45]. The peak energies at $\Delta t = 1$ ns are reasonably reproduced by those calculated by using Eq. (1) with $\delta_l = 0$, suggesting that the longer lifetime components are associated with Rydberg states belonging to the nl series such as the ng Rydberg series of Xe^+ which are identified up to $n = 22$ by threshold photoelectron

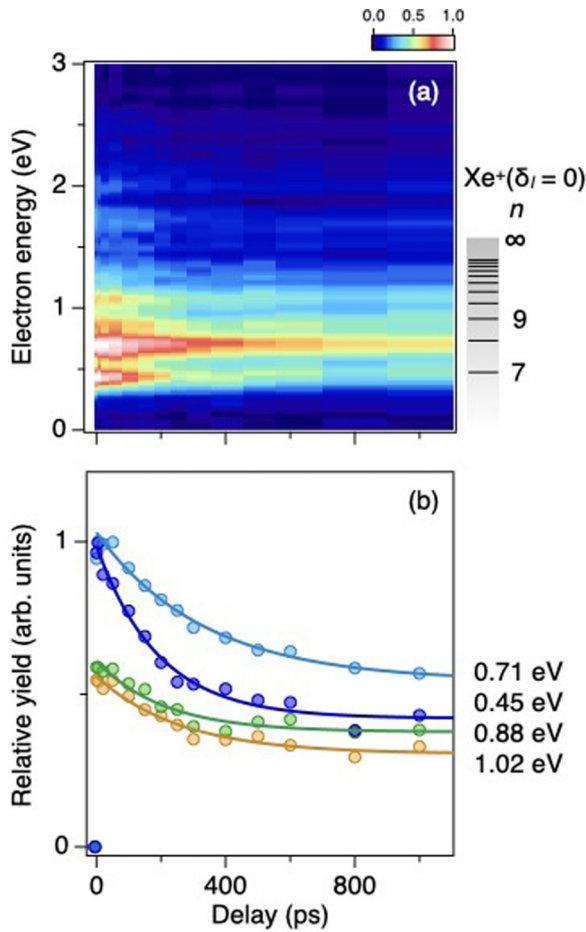


FIG. 4. (a) Pump-probe photoelectron spectra of Xe as a function of time delay between 0 and 1000 ps. Intensities of FEL and NIR pulses are the same as those in Fig. 3. (b) Time evolution of photoelectron peaks at 0.45 eV (blue), 0.71 eV (light blue), 0.88 eV (green), and 1.02 eV (orange). Solid curves represent single exponential functions (lifetime τ_1) fitted to the experimental data.

spectroscopy [18]. On the other hand, the subnanosecond decay components should be related to autoionization although ultrafast radiative decays of Rydberg states lying below the $\text{Xe}^{2+}(^3P_2)$ state cannot be ruled out. It should be noted that peaks at 0.88 and 1.02 eV are overlapped with autoionization peaks [β and γ in Fig. 3(a)] observed at the negative delays. In this case, the signal increase of these peaks is partially canceled by the decrease of the overlapping autoionization peaks due to ionization by NIR laser pulses, which may explain the smaller decay constants for the peaks at 0.88 and 1.02 eV than that for the peak at 0.71 eV.

To interrogate ultrafast decay for the sub-ps timescale, the timing monitor was employed at $\Delta t = 0$ ps. In this measurement, about 1.8×10^5 single-shot photoelectron spectra were collected with laser field intensities of 1.8×10^{14} W/cm² for EUV FEL and 4×10^{12} W/cm² for NIR. They were sorted in the order of the relative delay. Photoelectron signals below 0.5 eV were not detected in this measurement. Figures 5(a)–5(c) depict time evolution of the net photoelectron intensities at 0.71, 0.88, and 1.02 eV, respectively, obtained after subtraction of the background signals in the negative delay range between $\Delta t = -150$ fs and -50 fs. The time zero was set to the delay when the sideband of the Xe $5p$ photoelectron peak becomes the maximum (gray curve). Peaks at 0.71 and 0.88 eV clearly exhibit a transient signal reflecting ultrafast decay within ~ 100 fs while no clear decay is identified for the peak at 1.02 eV in the present time range. The decay component for the peak at 0.88 eV is smaller than that for 0.71 eV could be attributed to underestimation of the net signals discussed above.

We carried out numerical simulation based on coupled rate equations [36,46] for four-level model describing an indirect double ionization; state 1 is the ground state of Xe, state 2 is an autoionizing Rydberg state of Xe^+ with a lifetime (τ_2), state 3 is a Rydberg state of Xe^+ having no decay in this time range, and state 4 is a terminated state in Xe^{2+} [inset of Fig. 5(c)]. For simplicity, we assume that the probe process can be separated

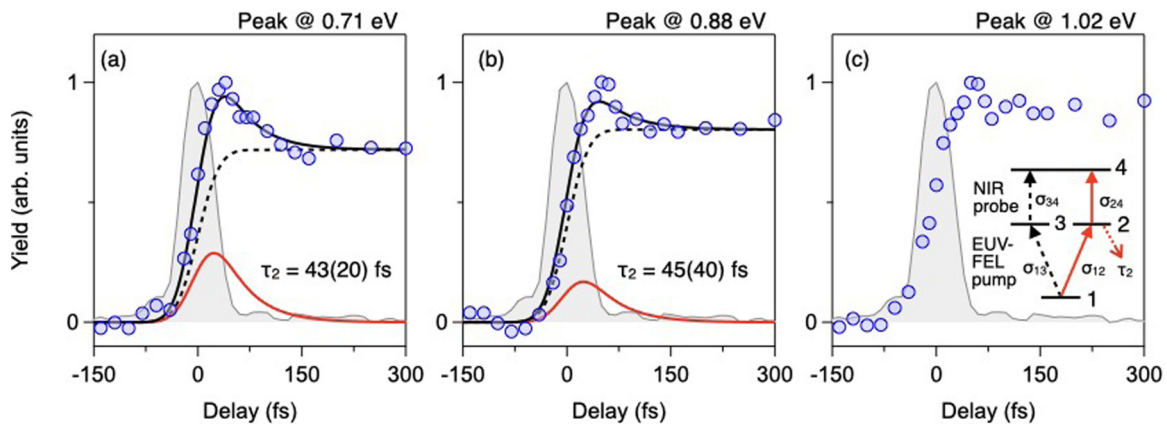


FIG. 5. Integrated intensities (circles) of photoelectron peak at (a) 0.71 eV, (b) 0.88 eV, and (c) 1.02 eV, as a function of time delay between EUV-FEL (1.8×10^{14} W/cm²) pump and NIR (4×10^{12} W/cm²) probe pulses. Pump-probe time delays were postcorrected using a timing monitor system. The time zero was determined by the maximum position of the transient signals of the Xe $5p$ photoelectron sideband (gray curve). Curves in (a,b) are obtained by fitting the integrated intensity data to simulated results based on coupled-rate equations for a four-level system depicted in the inset of (c). Dotted curve represents time dependence of a Rydberg state without decay while solid curve [red (gray)] depicts time evolution of an autoionizing state with a lifetime (τ_2). Solid curve (black) is the sum of these contributions.

from the pump process. Then the rate equations for the pump process could be expressed as

- (i) $dn_1(t)/dt = -\sigma_{12}I_{\text{FEL}}(t)n_1(t) - \sigma_{13}I_{\text{FEL}}(t)n_1(t)$,
- (ii) $dn_2(t)/dt = \sigma_{12}I_{\text{FEL}}(t)n_1(t) - (1/\tau_2)n_2(t)$,
- (iii) $dn_3(t)/dt = \sigma_{13}I_{\text{FEL}}(t)n_1(t)$,

where $n_i(t)$ stands for population of the i th state at time t , σ_{ij} for the ionization cross section from the i th state to the j th state, and $I_{\text{FEL}}(t)$ for the photon flux of the FEL pulse at time t . For the probe process, the ionization cross sections from state 3 and state 4 were assumed to be the same ($\sigma_{24} = \sigma_{34}$), so that the population of the terminated state [$n_4(t)$] is proportional to the sum of $n_2(t)$ and $n_3(t)$. The time-dependent population $n_i(t)$ is convoluted with the intensity profile of the NIR pulse. The FEL pump and NIR probe pulses were assumed to have Gaussian envelopes with a FWHM of 28 and 50 fs, respectively. To reproduce the observed time dependence in Fig. 5, the lifetime τ_2 and the cross-section ratio $A (= \sigma_{12}/\sigma_{13})$ were used as fitting parameters. The simulation was applied to the peaks at 0.71 and 0.88 eV. The experimental data were fitted with simulation curves by using a nonlinear least-squares method, and the optimized parameters were determined to be $\tau_2 = 43(20)$ fs, and $A = 0.9(2)$ for 0.71 eV and $\tau_2 = 45(40)$ fs, and $A = 0.5(3)$ for 0.88 eV. Simulated results for the Xe^{2+} state, autoionizing state, and the Xe^+ Rydberg state are depicted as solid black, solid red (gray), and dotted black curves, respectively.

The $(\text{Xe}^{2+} {}^1D) nd$ and $(\text{Xe}^{2+} {}^1S) nd$ Rydberg series of Xe^+ are known to undergo autoionization to the lower electronic states of Xe^{2+} [19] as is also observed in Fig. 3(a). In the present photon energy at 40.8 eV, the $(\text{Xe}^{2+} {}^1D) nd$ series are dominantly populated compared to the $(\text{Xe}^{2+} {}^1S) nd$ series while spectral widths of the $(\text{Xe}^{2+} {}^1D) nd$ series are narrower than those of the $(\text{Xe}^{2+} {}^1S) nd$ series [19]. These autoionizing states should be responsible for the present ultrafast decays with two different timescales of ~ 100 fs and ~ 300 ps. In addition to these two Rydberg series, Rydberg series converging to the excited $\text{Xe}^{2+} ({}^3P_0)$ and $\text{Xe}^{2+} ({}^3P_1)$ states could have some contribution for the decay components in the present study although autoionization from these states was not clearly identified in the previous study [19].

The lifetime of autoionizing levels varies by several orders of magnitude, depending on how they are coupled to the continuum state. Although less information on autoionization dynamics is available for singly charged ions, various relaxation processes for autoionizing states of neutral species have been reported. For instance, $5s$ correlation satellites of Xe in the $5s^15p^6({}^2S_{1/2})np$ ($n = 14-21$) and $5p^4({}^3P)6p({}^4D_{3/2})nd$ ($n = 10-13$) configurations resonantly excited by high-harmonic pulses are determined to be ~ 200 fs [47]. Longer lifetimes are reported for autoionizing Rydberg states ($n = 33-53$) lying between the lowest spin-orbit ${}^2P_{3/2}$ and ${}^2P_{1/2}$ levels of Xe [48], where wave-packet oscillations in the ps range are observed. Similarly, in the case of Ar atoms, lifetimes of the $3s3p^6np$ ($n = 4$ and 5) 1P states are estimated to be 8.2 and 23.3 fs [49] while those of the $np'[1/2]_0$ ($n = 11-16$) and $nf'[5/2]_2$ ($n = 9-11$) series converging to the $\text{Ar}^+ ({}^2P_{1/2})$ state fall in the ranges of 1–4 ps and 16–40 ps, respectively, according to the observed spectral widths [50]. Ultrashort lifetimes of Kr atoms are also identified as 140 fs

for the $4s4p^66p$ state [51] as well as 22, 33, and 49 fs for the $({}^2P_{1/2}) 6d/8s$, $({}^2P_{1/2}) 7d/9s$, and $({}^2P_{1/2}) 8d/10s$ states [52], respectively. In either case above, spin-orbit interactions play a key role in the autoionization process.

In the present autoionization of Xe^{+*} , the $(\text{Xe}^{2+} {}^1D) nd (n > 8)$ Rydberg states decay into the 3P manifolds of Xe^{2+} with almost its statistical ratio while $(\text{Xe}^{2+} {}^1S) nd (n > 9)$ Rydberg states lying above the $\text{Xe}^{2+} ({}^1D_2)$ ionization threshold autoionize preferentially to the 1D_2 state rather than to the 3P manifolds [19]. The transition from the singlet to triplet states in the ion core indicates also the importance of taking into account the spin-orbit interaction in the description of autoionization processes of the $(\text{Xe}^{2+} {}^1D) nd (n > 8)$ Rydberg states in contrast to those of $(\text{Xe}^{2+} {}^1S) nd (n > 9)$ Rydberg states. The two distinct decay constants of ~ 100 fs and ~ 300 ps observed in the present study suggest that the corresponding autoionizing states have different coupling schemes to the continuum. Identification of the detailed mechanism is beyond of the scope of the current study and requires a theoretical calculation taking into account appropriate configuration interactions for heavy atoms.

IV. SUMMARY

We have employed ultrafast photoelectron spectroscopy of the Rydberg states of Xe^+ lying above the double-ionization threshold by using EUV-FEL and NIR laser pulses. Time-resolved photoelectron spectra in the fs and ps time resolutions revealed a slight decay with a lifetime of ~ 100 fs followed by a subsequent decay within several hundreds ps. The ultrafast decays are attributed to autoionizing states belonging to the $(\text{Xe}^{2+} {}^1D) nd$ and $(\text{Xe}^{2+} {}^1S) nd$ Rydberg series. Photoelectron peaks lasting 1 ns are associated with Rydberg series having negligible quantum defects of Xe^+ converging to the lowest $\text{Xe}^{2+} ({}^3P_2)$ threshold. Although these Rydberg series exhibit almost the same photoelectron spectral width due to the limited instrumental resolution, Rydberg series having different lifetimes can be distinguished by inspecting the time evolution of the photoelectron signals. The present work demonstrates that the time resolution beyond the jitter limitation allows for investigating ultrafast electron dynamics associated with indirect double ionization which provides complementary information against the high-resolution spectroscopy in the frequency domain.

ACKNOWLEDGMENTS

We thank the operation and engineering staff members of SACLA for their support on this work. The experiments were conducted at SACLA BL1 with the approval of the Japan Synchrotron Radiation Research Institute (JASRI) (Proposals No. 2016B8018, No. 2017B8081, No. 2018B8028, and No. 2020A8049). This work is partially supported by JSPS KAKENHI (Grants No. JP18K03489 and No. JP20K05549), World Research Unit (B-1) of Reaction Infography (R-ing) at Nagoya University, and Morino Foundation for Molecular Science.

- [1] J. H. D. Eland, *Chem. Phys.* **294**, 171 (2003).
- [2] A. Huetz, P. Selles, D. Waymel, and J. Mazeau, *J. Phys. B* **24**, 1917 (1991).
- [3] A. Lahmam-Bennani, *J. Phys. B* **24**, 2401 (1991).
- [4] J. H. McGuire, N. Berrah, R. J. Bartlett, J. A. R. Samson, J. A. Tanis, C. L. Cocke, and A. S. Schlachter, *J. Phys. B* **28**, 913 (1995).
- [5] L. Avaldi and A. Huetz, *J. Phys. B* **38**, S861 (2005).
- [6] B. Krässig, S. J. Schaphorst, O. Schwarzkopf, N. Scherer, and V. Schmidt, *J. Phys. B* **29**, 4255 (1996).
- [7] J. Mazeau, P. Lablanquie, P. Selles, L. Malegat, and A. Huetz, *J. Phys. B* **30**, L293 (1997).
- [8] M. Jurvansuu, A. Kivimäki, and S. Aksela, *Phys. Rev. A* **64**, 012502 (2001).
- [9] G. B. Armen, H. Aksela, T. Åberg, and S. Aksela, *J. Phys. B* **33**, R49 (2000).
- [10] D. Proulx and R. Shakeshaft, *Phys. Rev. A* **48**, R875 (1993).
- [11] G. Dujardin, M. J. Besnard, L. Hellner, and Y. Malinovitch, *Phys. Rev. A* **35**, 5012 (1987).
- [12] M. Gisselbrecht, M. Lavollée, A. Huetz, P. Bolognesi, L. Avaldi, D. P. Seecombe, and T. J. Reddish, *Phys. Rev. Lett.* **96**, 153002 (2006).
- [13] M. Carlsson-Gothe, P. Baltzer, and B. Wannberg, *J. Phys. B* **24**, 2477 (1991).
- [14] A. Kikas, S. J. Osborne, A. Ausmees, S. Svensson, O. P. Sairanen, and S. Aksela, *J. Electron Spectrosc. Relat. Phenom.* **77**, 241 (1996).
- [15] B. M. Lagutin, I. D. Petrov, V. L. Sukhorukov, S. B. Whitfield, B. Langer, J. Viefhaus, R. Wehlitz, N. Berrah, W. Mahler, and U. Becker, *J. Phys. B* **29**, 937 (1996).
- [16] A. E. Slattery, J. P. Wightman, M. A. MacDonald, S. Cvejanovic, and T. J. Reddish, *J. Phys. B* **33**, 4833 (2000).
- [17] S. Alitalo, A. Kivimäki, T. Matila, K. Vaarala, H. Aksela, and S. Aksela, *J. Electron Spectrosc. Relat. Phenom.* **114–116**, 141 (2001).
- [18] H. Yoshii, T. Aoto, Y. Morioka, and T. Hayaishi, *J. Phys. B* **40**, 2765 (2007).
- [19] J. H. D. Eland, O. Vieuxmaire, T. Kinugawa, P. Lablanquie, R. I. Hall, and F. Penent, *Phys. Rev. Lett.* **90**, 053003 (2003).
- [20] D. Waymel, L. Andric, I. Mazeau, P. Selles, and A. Huetz, *J. Phys. B* **26**, L123 (1993).
- [21] M. Böttcher, H. Rottke, N. Zhavoronkov, W. Sandner, P. Agostini, M. Gisselbrecht, and A. Huetz, *J. Phys. B* **38**, L389 (2005).
- [22] O. Guyétand, M. Gisselbrecht, A. Huetz, P. Agostini, B. Carré, P. Breger, O. Gobert, D. Garzella, J. F. Hergott, O. Tcherbakoff, H. Merdji, M. Bougeard, H. Rottke, M. Böttcher, Z. Ansari, P. Antoine, and L. F. DiMauro, *J. Phys. B* **41**, 065601 (2008).
- [23] M. Böttcher, H. Rottke, N. Zhavoronkov, W. Sandner, P. Agostini, M. Gisselbrecht, and A. Huetz, *Phys. Rev. A* **75**, 033408 (2007).
- [24] E. P. Månsson, D. Guénot, C. L. Arnold, D. Kroon, S. Kasper, J. M. Dahlström, E. Lindroth, A. S. Kheifets, A. L'Huillier, S. L. Sorensen, and M. Gisselbrecht, *Nat. Phys.* **10**, 207 (2014).
- [25] J. M. Bizau, F. Wuilleumier, D. L. Ederer, J. C. Keller, J. L. LeGouët, J. L. Picqué, B. Carré, and P. M. Koch, *Phys. Rev. Lett.* **55**, 1281 (1985).
- [26] M. Meyer, M. Gisselbrecht, A. Marquette, C. Delisle, M. Larzillière, I. D. Petrov, N. V. Demekhina, and V. L. Sukhorukov, *J. Phys. B* **38**, 285 (2005).
- [27] M. Meyer, B. Müller, A. Nunnemann, T. Prescher, E. v. Raven, M. Richter, M. Schmidt, B. Sonntag, and P. Zimmermann, *Phys. Rev. Lett.* **59**, 2963 (1987).
- [28] M. Fushitani, Y. Hikosaka, A. Matsuda, T. Endo, E. Shigemasa, M. Nagasono, T. Sato, T. Togashi, M. Yabashi, T. Ishikawa, and A. Hishikawa, *Phys. Rev. A* **88**, 063422 (2013).
- [29] S. Minemoto, H. Shimada, K. Komatsu, W. Komatsubara, T. Majima, S. Miyake, T. Mizuno, S. Owada, H. Sakai, T. Togashi, M. Yabashi, P. Decleva, M. Stener, S. Tsuru, and A. Yagishita, *J. Phys. Commun.* **2**, 115015 (2018).
- [30] P. Radcliffe, S. Düsterer, A. Azima, W. B. Li, E. Plönjes, H. Redlin, J. Feldhaus, P. Nicolosi, L. Poletto, J. Dardis, J. P. Gutierrez, P. Hough, K. D. Kavanagh, E. T. Kennedy, H. Luna, P. Yeates, J. T. Costello, A. Delyseries, C. L. S. Lewis, D. Glijer *et al.*, *Nucl. Instrum. Methods Phys. Res., Sect. A* **583**, 516 (2007).
- [31] K. Schnorr, A. Senftleben, G. Schmid, A. Rudenko, M. Kurka, K. Meyer, L. Foucar, M. Kübel, M. F. Kling, Y. H. Jiang, S. Düsterer, R. Treusch, C. D. Schröter, J. Ullrich, T. Pfeifer, and R. Moshhammer, *Faraday Discuss.* **171**, 41 (2014).
- [32] A. Azima, S. Düsterer, P. Radcliffe, H. Redlin, N. Stojanovic, W. Li, H. Schlarb, J. Feldhaus, D. Cubaynes, M. Meyer, J. Dardis, P. Hayden, P. Hough, V. Richardson, E. T. Kennedy, and J. T. Costello, *Appl. Phys. Lett.* **94**, 144102 (2009).
- [33] M. Drescher, U. Frühling, M. Krikunova, T. Maltezopoulos, and M. Wieland, *J. Phys. B* **43**, 194010 (2010).
- [34] J. M. Glowia, J. Cryan, J. Andreasson, A. Belkacem, N. Berrah, C. I. Blaga, C. Bostedt, J. Bozek, L. F. DiMauro, L. Fang, J. Frisch, O. Gessner, M. Gühr, J. Hajdu, M. P. Hertlein, M. Hoener, G. Huang, O. Kornilov, J. P. Marangos, A. M. March *et al.*, *Opt. Express* **18**, 17620 (2010).
- [35] S. Owada, M. Fushitani, A. Matsuda, H. Fujise, Y. Sasaki, Y. Hikosaka, A. Hishikawa, and M. Yabashi, *J. Synchrotron Radiat.* **27**, 1362 (2020).
- [36] Y. Hikosaka, M. Fushitani, A. Matsuda, C.-M. Tseng, A. Hishikawa, E. Shigemasa, M. Nagasono, K. Tono, T. Togashi, H. Ohashi, H. Kimura, Y. Senba, M. Yabashi, and T. Ishikawa, *Phys. Rev. Lett.* **105**, 133001 (2010).
- [37] K. Nagaya, T. Sakai, T. N. Hiraki, S. Yase, K. Matsunami, K. Asa, H. Fukuzawa, K. Motomura, Y. Kumagai, W. Q. Xu, S. Wada, H. Hayashita, N. Saito, M. Nagasono, T. Togashi, M. Yabashi, and K. Ueda, *J. Phys. Commun.* **5**, 015014 (2021).
- [38] E. Kukk, H. Fukuzawa, J. Niskanen, K. Nagaya, K. Kooser, D. You, J. Peschel, S. Maclot, A. Niozu, S. Saito, Y. Luo, E. Pelimanni, E. Itälä, J. D. Bozek, T. Takanashi, M. Berholts, P. Johnsson, and K. Ueda, *Phys. Rev. Research* **3**, 013221 (2021).
- [39] M. B. Danailov, F. Bencivenga, F. Capotondi, F. Casolari, P. Cinquegrana, A. Demidovich, E. Giangrisostomi, M. P. Kiskinova, G. Kurdi, M. Manfredda, C. Masciovecchio, R. Mincigrucchi, I. P. Nikolov, E. Pedersoli, E. Principi, and P. Sigalotti, *Opt. Express* **22**, 12869 (2014).
- [40] M. Fushitani, S. T. Pratt, D. You, S. Saito, Y. Luo, K. Ueda, H. Fujise, A. Hishikawa, H. Ibrahim, F. Légaré, P. Johnsson, J. Peschel, E. R. Simpson, A. Olofsson, J. Mauritsson, P. A. Carpeggiani, P. K. Maroju, M. Moiola, D. Ertel, R. Shah *et al.*, *J. Chem. Phys.* **154**, 144305 (2021).
- [41] M. Fushitani and A. Hishikawa, *Struct. Dyn.* **3**, 062602 (2016).
- [42] M. Fushitani, Y. Toida, F. Légaré, and A. Hishikawa, *Opt. Express* **27**, 19702 (2019).

- [43] T. X. Carroll, J. D. Bozek, E. Kukk, V. Myrseth, L. J. Saethre, T. D. Thomas, and K. Wiesner, *J. Electron Spectrosc. Relat. Phenom.* **125**, 127 (2002).
- [44] I. D. Petrov, V. L. Sukhorukov, and H. Hotop, *J. Phys. B* **35**, 323 (2002).
- [45] K. Blagoev, N. Dimitrov, and M. Drenska, *J. Phys. B* **17**, 2189 (1984).
- [46] M. Fushitani, Y. Sasaki, A. Matsuda, H. Fujise, Y. Kawabe, K. Hashigaya, S. Owada, T. Togashi, K. Nakajima, M. Yabashi, Y. Hikosaka, and A. Hishikawa, *Phys. Rev. Lett.* **124**, 193201 (2020).
- [47] M. Baggash and H. Rottke, *Phys. Rev. A* **91**, 053403 (2015).
- [48] J. A. Ramswell, V. G. Stavros, J. Lei, Q. Hong, and H. H. Fielding, *Phys. Rev. A* **59**, 2186 (1999).
- [49] H. Wang, M. Chini, S. Chen, C.-H. Zhang, F. He, Y. Cheng, Y. Wu, U. Thumm, and Z. Chang, *Phys. Rev. Lett.* **105**, 143002 (2010).
- [50] Y.-Y. Lee, T.-Y. Dung, R.-M. Hsieh, J.-Y. Yuh, Y.-F. Song, G. H. Ho, T.-P. Huang, W.-C. Pan, I.-Chia Chen, S.-Y. Tu, A. H. Kung, and L. C. Lee, *Phys. Rev. A* **78**, 022509 (2008).
- [51] B. Doughty, L. H. Haber, C. Hackett, and S. R. Leone, *J. Chem. Phys.* **134**, 094307 (2011).
- [52] A. P. Fidler, H. J. B. Marroux, E. R. Warrick, E. Bloch, W. Cao, S. R. Leone, and D. M. Neumark, *J. Chem. Phys.* **151**, 114305 (2019).